physchem

MDPI

Article

Utilizing Residual Industrial Waste as Sustainable Adsorbents for the Removal of Indigo Carmine from Contaminated Water

Amina Ghedjemis [1,2], Maya Kebaili [3,4], Kamel Hebbache [5], Cherif Belebchouche [5,*] and El Hadj Kadri [6,*]

[1] Department of Sciences, Teacher Education College of Setif—Messaoud Zeghar, El Eulma 19600, Algeria; a.ghedjemis@ens-setif.dz
[2] Laboratory of Characterization, Valorization of Natural Resources, Mohamed El Bachir El Ibrahim University, Bordj Bou Arreridj 34030, Algeria
[3] Mechanics Research Center (CRM), BP N73B, Frères Ferrad, Ain El Bey, Constantine 25021, Algeria
[4] Unit of Research in Nanosciences and Nanotechnologies (URNN), Center for Development of Advanced Technologies (CDTA), Setif 1 University-Ferhat Abbas, Setif 19000, Algeria
[5] Civil Engineering Research Laboratory of Sétif (LRGCS), Department of Civil Engineering, Setif 1 University-Ferhat Abbas, Setif 19000, Algeria; hebbache.kamel@univ-setif.dz
[6] Mechanics and Civil Engineering Materials Laboratory (L2MGC), University of CY-Paris, 95031 Cergy-Pontoise, France
* Correspondence: cherif.belebchouche@univ-setif.dz (C.B.); pr.elhadj.kadri@gmail.com (E.H.K.)

Abstract: The recovery of green waste and biomass presents a significant challenge in the 21st century. In this context, this study aims to valorize waste generated by the fruit juice processing industry at the N'Gaous unit (composed of the orange peel, fibers, pulp, and seeds) as an adsorbent to eliminate an anionic dye and to enhance its adsorption capacity through thermal activation at 200 °C and 400 °C. The aim is also to determine the parameters for the adsorption process including contact time (0–120 min), solution pH (2–10), initial dye concentration (50–700 mg/L), and adsorbent dosage (0.5–10 g/L). The adsorption tests showed that waste activated at 400 °C (AR400) demonstrated a higher efficiency for removing indigo carmine (IC) from an aqueous solution than waste activated at 200 °C (AR200) and unactivated waste (R). The experimental maximum adsorption capacities for IC were 70 mg/g for unactivated waste, 500 mg/g for waste activated at 200 °C, and 680 mg/g for waste activated at 400 °C. These tests were conducted under conditions of pH 2, an equilibrium time of 50 min, and an adsorbent concentration of 1 g/L. The analysis of the kinetic data revealed that the pseudo-second-order model provides the best fit for the experimental results, indicating that this mechanism predominates in the sorption of the pollutant onto the three adsorbents. In terms of adsorption isotherms, the Freundlich model was found to be the most appropriate for describing the adsorption of dye molecules on the R, AR200, and AR400 supports, owing to its high correlation coefficient. Before adsorption tests, the powder R, AR200 and AR400 were characterized by various analyses, including Fourier transform infrared (FTIR), pH zero charge points and laser granularity for structural evaluation. According to the results of these analyses, the specific surface area (SSA) of the prepared material increases with the increase in the activation temperature, which expresses the increase in the adsorption of material activated at 400 °C, compared with materials activated at 200 °C and the raw material.

Keywords: adsorption; indigo carmine; industrial juice waste; activated industrial juice waste

check for updates

Academic Editor: Sergei Manzhos

Received: 23 February 2025
Revised: 27 May 2025
Accepted: 28 May 2025
Published: 29 May 2025

Citation: Ghedjemis, A.; Kebaili, M.; Hebbache, K.; Belebchouche, C.; Kadri, E.H. Utilizing Residual Industrial Waste as Sustainable Adsorbents for the Removal of Indigo Carmine from Contaminated Water. *Physchem* **2025**, *5*, 21. https://doi.org/10.3390/physchem5020021

Copyright: © 2025 by the authors. Licensee MDPI, Basel, Switzerland. This article is an open access article distributed under the terms and conditions of the Creative Commons Attribution (CC BY) license (https://creativecommons.org/licenses/by/4.0/).

1. Introduction

Orange cultivation is a crucial agricultural activity in many countries around the world [1], valued of its high demand in diverse applications, high nutritional component and health benefits [2]. The Oranges fruit (scientific name) is commonly used in different industries, as a fundamental ingredient in food and beverages, cosmetics, cleaning products, and essential oil production because of their natural flavors and antibacterial properties [3]. In alternative medicine, oranges and their essential oils are regarded as beneficial for stimulating the immune system and treating colds, primarily due to their high vitamin C content and antioxidants [4,5].

Global orange production is continually rising as many countries are adopting modern agricultural technologies and expanding the land dedicated to citrus cultivation [6]. This growth has resulted in increased production, helping to meet the demands of both local and international markets of the leading orange-producing countries in the world such as Brazil, the United States, and India [7]. In recent years, orange production in Algeria has experienced significant growth, reflecting the importance of agriculture to the national economy [8]. The country's moderate climate, particularly in coastal areas, creates an ideal environment for cultivating citrus fruits such as oranges [9]. Algeria is concentrating on improving production quality and increasing planted quantities to meet local demand and export the surplus. This growth in production has contributed to a reduction in orange prices in the markets, making them more affordable for various segments of society [10]. Resulting to agricultural policies and improved distribution networks, oranges have become a vital part of the daily diet in Algeria and around the world. However, the large production of this fruit has resulted in significant secondary waste, particularly from juice production facilities. The waste primarily consists of peels, seeds, fibers, and pulp, which are often used as animal feed [11,12]. Unfortunately, these byproducts are considered harmful and ineffective for animal consumption, creating challenges for factories in terms of storage, collection, and disposal. This situation poses an increasing risk of environmental pollution, which is a direct threat to human health Finding innovative ways to dispose of waste from orange juice factories and to repurpose it into profitable ventures is a crucial step toward achieving both environmental and economic sustainability [13]. Instead of being discarded as waste that harms the environment and emits greenhouse gases during decomposition, this waste can be transformed into valuable economic resources [14].

As known, water is one of the most important renewable natural resources and is essential for the continuation of life on Earth. It is considered the lifeblood of humans, plants, and animals. However, water has become increasingly vulnerable to pollution due to rising human activities, which poses a serious threat to the environment and public health [15,16]. One of the most dangerous types of water pollution is caused by factory waste, particularly chemicals like heavy metals (such as lead, mercury, and cadmium) and industrial dyes [15]. Dyes can change the color of water, reduce light penetration, and have harmful effects on plants and marine organisms. Indigo Carmine, one of the synthetic anionic dyes plays a significant role in various industrial applications due to its strong dyeing properties. It is extensively employed in the textile industry for fabric coloration, in the food sector as an additive (E132), and in the medical field as a contrast agent for specific diagnostic procedures. However, despite its broad utility, growing concerns have emerged regarding its potential health and environmental risks. Recent studies have reported that exposure to indigo carmine may induce adverse effects, including allergic reactions, cardiovascular disorders, and potential genotoxicity. Furthermore, its persistence in industrial effluents raises ecological concerns, particularly regarding its impact on aquatic ecosystems [17]. To protect water as a sustainable resource, it is essential to implement strict measures to reduce pollution [18]. Key strategies include enhancing industrial

water treatment systems before wastewater is discharged. The most important treatment methods are: physical methods (Filtration, Adsorption, Sedimentation and Coagulation), Chemical Methods (Oxidation and Electrocoagulation) and Biological Methods (Microbial Degradation, Phytoremediation and Enzymatic Treatment) [19].

Adsorption is a widely used and effective technique for treating water contaminated by industrial dyes [20]. This method uses the ability of an adsorbent to capture and adhere to dye molecules on its surface, thereby reducing their concentration in water. Its popularity stems from its simplicity, relatively low cost, and effectiveness in removing even low concentrations of dyes. Adsorption is applied in various industries, including textiles, paper, and cosmetics, where dyes are a significant source of pollution [18]. There is a wide range of adsorbents available, such as synthetic materials and natural options like activated carbon, natural clay, and zeolite, as well as biosorbants like fungi and algae [20].

The aim of this study is to investigate the waste collected from orange juice N'Gaous factories, which is composed by the orange peel, fibers, pulp, and seeds as adsorbent and thermally treat. This waste to increase its adsorption capacity for the removal of anionic dyes from water, in order to reduce water pollution. This innovative approach seeks to fully use these residues, which is an area that remains largely unexplored. Existing studies typically focus on only one part of this waste, whereas this research aims to consider the complete exploitation of all components.

2. Materials and Methods

2.1. Adsorbent Treatment

The adsorbent used in this research is the waste generated by the fruit juice processing industry at the N'Gaous unit, consisting mainly of orange peels, fibers, pulp, and seeds. During the juice production process in the factory, the fruit undergoes multiple rinsing stages as it passes through the press. This procedure ensures the complete removal of soluble sugars from the waste, leaving only insoluble sugars in the residue, which is used as the adsorbent. This waste is dried in an oven for 2 h at 105 °C and then milled using a ball mill (Retsch) at a ratio of 1/10 beads, the grinding speed is set to 300 rpm for a duration of 20 min, it is the raw adsorbent R. The raw adsorbent is activated by heat-treatment by a muffle furnace in normal (atmospheric) air at different temperatures at 200 °C (AR200) and at 400 °C (AR400) for 1 h with a heating rate of 10 °C/min.

2.2. Characterization of the Adsorbent

2.2.1. Point of Zero Charge

The point of zero charge (pH_{PZC}) was measured using the methodology established by Vieira et al. The experimental method involves introducing 100 mL of distilled water into hermetically sealed flasks. The initial pH of the solutions is adjusted to values between 2 and 10 using 0.1 M solutions of NaOH or HCl. To each flask, 0.01 g of the samples (R, AR200 and AR400) to be characterized is added. The resulting suspensions are continuously stirred at room temperature for 24 h. After this period, the final pH of the supernatants is measured. The variation in pH ($\Delta pH = pH0 - pHf$) is then plotted as a function of the initial pH (pH_0). The point of intersection where the pH variation is zero indicates the point of zero charge (pH_{PZC}) [21].

2.2.2. Fourier Transform Infrared Spectroscopy (FTIR) Analysis

At this analysis was conducted to identify the primary functional groups present on the surface of the adsorbents (R, AR200 and AR400). These functional groups are crucial for the chemical and physical interactions that occur during the adsorption process.

2.2.3. Laser Granularity Analysis

The crushed samples (R, AR200 and AR400) were analyzed using laser granularity (Cilas Particle Size Analyzer 1090, KWIPPED, Wilmington, DE, USA) to evaluate the impact of temperature on their particle size distribution and surface characteristics.

2.3. Adsorption Test

The adsorption of indigo carmine (IC) as anionic dye onto the raw waste (R), activated at 200 °C (AR200) and activated at 400 °C (AR400) was investigated through a series of batch experiments. The ideal conditions for maximizing adsorption capacity were identified through a systematic analysis of the factors influencing the adsorption process. A dye solution of IC (50 mg/L) were prepared by dissolving the dye powder in distilled water and then diluting it to create a concentration range of 25 to 50 mg/L. The effects of several experimental parameters including contact time (0–120 min), pH (2, 4, 6, 8 and 10), and adsorbent dose (0.5–10 g/L) were explored by varying one parameter at a time while keeping the others constant. The experiments were conducted in 250 mL conical flasks containing 100 mL of the dye solution, with precise pH adjustments made using hydrochloric acid (0.1 M) and sodium hydroxide (0.1 M) solutions. After shaking, the samples were centrifuged at 4000 rpm for 10 min using a Sigma 3–30 KS centrifuge. The concentration of the remaining dye in the supernatant was measured with a Secomam Uviline 9400 UV-Vis spectrophotometer at a wavelength of 608 nm. The amount of IC adsorbed per unit mass of adsorbent was calculated using the following Equation (1):

$$q_t = \frac{(C_0 - C_t)V}{W} \quad (1)$$

where, q_t, C_0, C_t, V, and W are the quantity adsorbed at time t (mg/g), the initial concentration (mg/L), the concentration at time t (mg/L), the solution volume (L), and the adsorbent mass (g), respectively.

3. Results and Discussion

3.1. This Characterization of the Adsorbent

3.1.1. The pH Zero Charge Point

This measurement helps us understand the surface charge properties of adsorbents. It indicates the pH at which the adsorbent surface has a net zero charge, providing important insights into the electrostatic behavior of the adsorbent across different pH conditions. This information is crucial for understanding the mechanisms of adsorption and the interaction with ions in solution. In simpler terms, it specifies the pH level at which the surface of the adsorbent becomes either positively or negatively charged, thereby affecting its interactions with ionic species in solution.

The results shown in Figure 1, clearly illustrate the pH zero charge point (pHpzc) for the three adsorbents studied: raw waste (R), activated at 200 (AR200) and activated at 400 °C (AR400). The pHpzc values obtained are respectively 4.5, 5 and 9.

Thermal activation generally increases the porosity and surface area of lignocellulosic materials, which can expose new active sites and influence the distribution and accessibility of surface charges [22].

An increase in surface area may amplify the overall surface reactivity and affect the protonation/deprotonation behavior of the functional groups, thereby influencing the pHpzc.

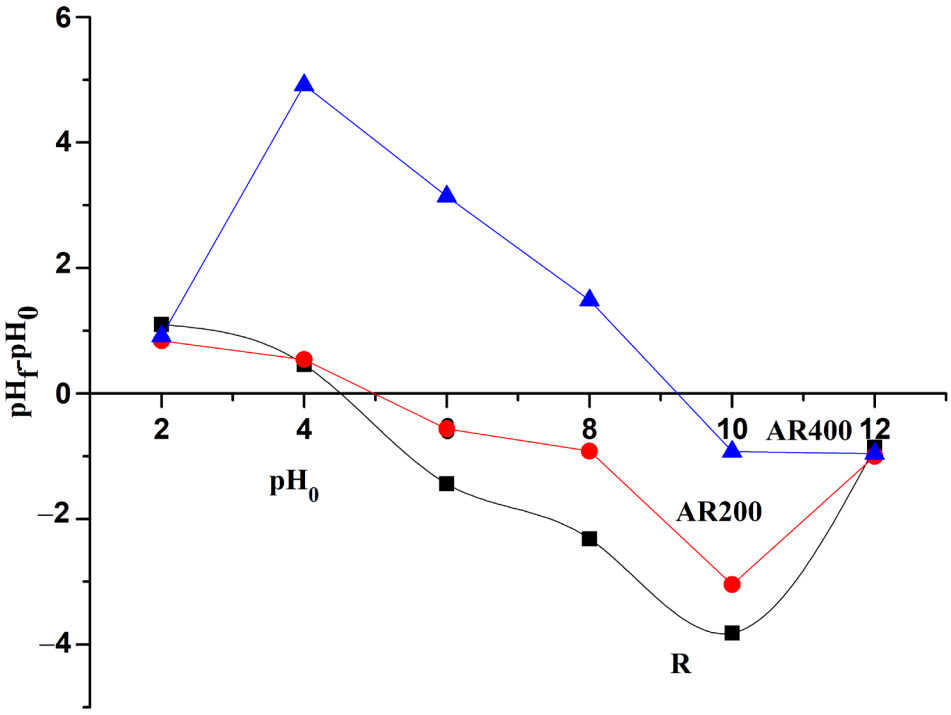


Figure 1. The zero-potential charge point (pHZPC) of: R, AR200 and AR400.

3.1.2. Fourier Transform Infrared Spectroscopy (FTIR) Results

To enhance our understanding of the surface functions of residues from the orange industry, both in their raw waste and activated state, we analyzed their structures using infrared spectroscopy. The infrared spectra for the untreated and activated materials are displayed in Figure 2. In the raw material (R), a broad band centered around 3350 cm^{-1} is prominent, attributed to O-H stretching vibrations. This encompasses contributions from adsorbed water, hydroxyl groups in cellulose, hemicellulose, and lignin, as well as phenolic -OH groups [23,24]. The intensity of this band progressively decreases in the order R > AR200 > AR400, which clearly indicates substantial dehydration and dehydroxylation during thermal activation [25]. Aliphatic C-H stretching vibrations are evident from peaks at approximately 2932 cm^{-1} (asymmetric CH_2, CH_3) and 2880 cm^{-1} (symmetric CH_2, CH_3), primarily originating from cellulose and hemicellulose chains, and to a lesser extent, lipids [26]. The diminishing intensity of these bands, particularly in AR400, reflects the cleavage and volatilization of these aliphatic structures.

An absorption, often appearing as a shoulder around 1735–1740 cm^{-1} in R and AR200, is characteristic of C=O stretching in ester groups and non-conjugated carboxylic acids [27]. Its near disappearance in AR400 signifies extensive de-esterification and decarboxylation. The band around 1630 cm^{-1} is multifaceted: in R, it is significantly influenced by O-H bending vibrations of adsorbed water. With increasing activation temperature (AR200, AR400), contributions from C=C stretching in aromatic rings [28,29]. The relative stability or slight intensification of this band in AR400, despite the loss of other functionalities, points to a relative enrichment of these thermally stable (poly) aromatic carbon structures.

Absorptions in the 900–700 cm^{-1} range, such as the band around 750 cm^{-1}, are typically associated with C-H out-of-plane bending vibrations of aromatic rings. In R, these originate from lignin. In AR200 and AR400, an increase in the relative intensity or shifts in this region can indicate the development and condensation of polyaromatic structures within the char [30].

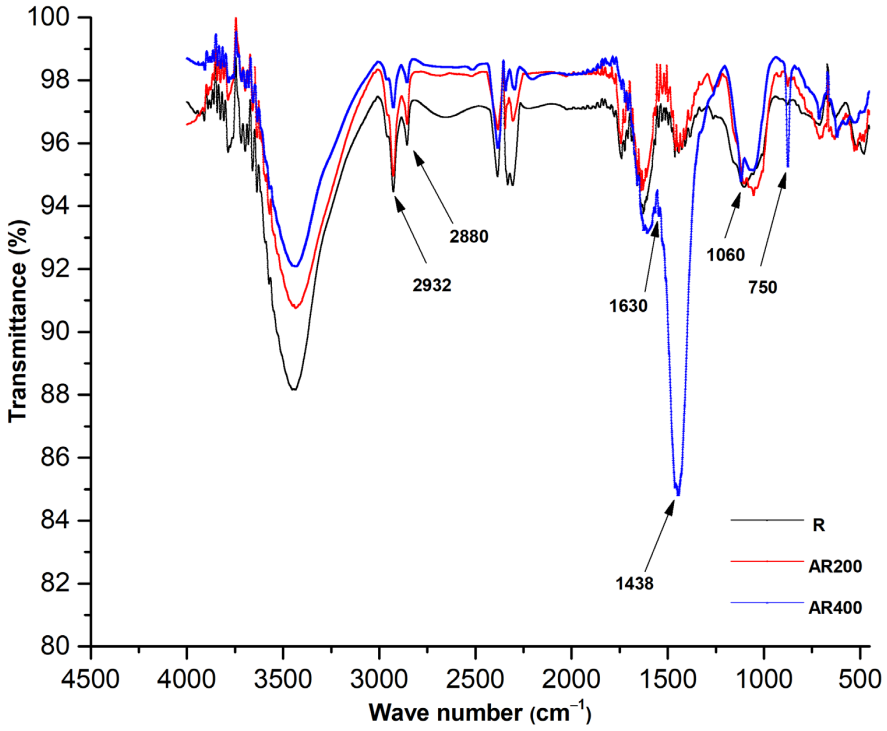


Figure 2. Fourier transform infrared spectroscopy of adsorbents: R, AR200 and AR400.

Overall, the FTIR spectra clearly show that thermal activation induces profound chemical changes. Increasing temperature leads to the loss of hydroxyl, aliphatic, and polysaccharide functional groups. Concurrently, there is a relative enrichment of aromatic structures and, at 400 °C, significant formation of inorganic carbonates. These alterations in surface chemistry, particularly the varying abundance of oxygen-containing functional groups (hydroxyl, carboxyl implied by C-O loss), directly influence surface properties and are consistent with expected changes in characteristics like the point of zero charge (pHpzc) [22].

3.1.3. Laser Granularity Results

The results of the laser particle size analysis indicate that temperature affects the particle size of the sample. There is a negative correlation between temperature and the particle size of the powder prepared from the waste generated by the fruit juice processing industry. The average particle sizes are as follows: 180.43 µm for R, 120.26 µm for AR200, and 60.12 µm for AR400. Correspondingly, the average specific surface area (SSA) are 5.23 m^2/g for R, 8 m^2/g for AR200, and 12.54 m^2/g for AR400. These results demonstrate a positive correlation between temperature and particle-specific surface area for R, AR200, and AR400.

3.2. Adsorption Results

3.2.1. Effect of Initial pH

The pH of the dye solution is a crucial factor that influences the adsorption process, particularly the retention capacity of the adsorbates. The solution's pH affects not only the surface charge of the adsorbent but also the degree of ionization of the dyes and the dissociation of functional groups on the active sites of the adsorbent. Additionally, it plays a significant role in the chemistry of the dyes in the solution.

Hydrogen (H+) and hydroxyl (OH-) ions interact strongly with the adsorbent surface, impacting the adsorption of other ions present. Generally, it is accepted that anionic dyes are more effectively adsorbed at acidic pH levels due to the presence of ions that

neutralize the negative charges on the adsorbent surface. Conversely, cationic dyes are preferentially adsorbed at alkaline pH levels because the adsorbent surface acquires a negative charge [31,32].

The illustrated results in Figure 3, demonstrate that the adsorption capacity of Indigo Carmine (IC) on R, AR200 and AR400 shows significant variation with pH levels. The adsorption of IC onto the surface of three samples is less effective in alkaline conditions due to an increase in negative charges on the surface. In contrast, adsorption is more favorable in acidic conditions. This behavior can be attributed to the electrostatic interactions between the positively functional groups on the surface of samples and the anion groups present in IC (Figure 4). These findings confirm the strong correlation between pHpzc and solution pH which when the solution pH is below pHpzc, the surface of the adsorbent becomes positively charged, promoting the adsorption of anionic species such as Indego Carmine (IC) due to electrostatic attraction. Conversely, when the pH is above pHpzc, the surface acquires negative charges, leading to electrostatic repulsion and reduced adsorption capacity. Since the maximum adsorption capacity (q_{max}) occurs at a pH of 2 is 19.85, 25.87, 30 mg/g for R, AR200 and AR400, respectively. This pH was chosen as the optimal value for subsequent adsorption tests.

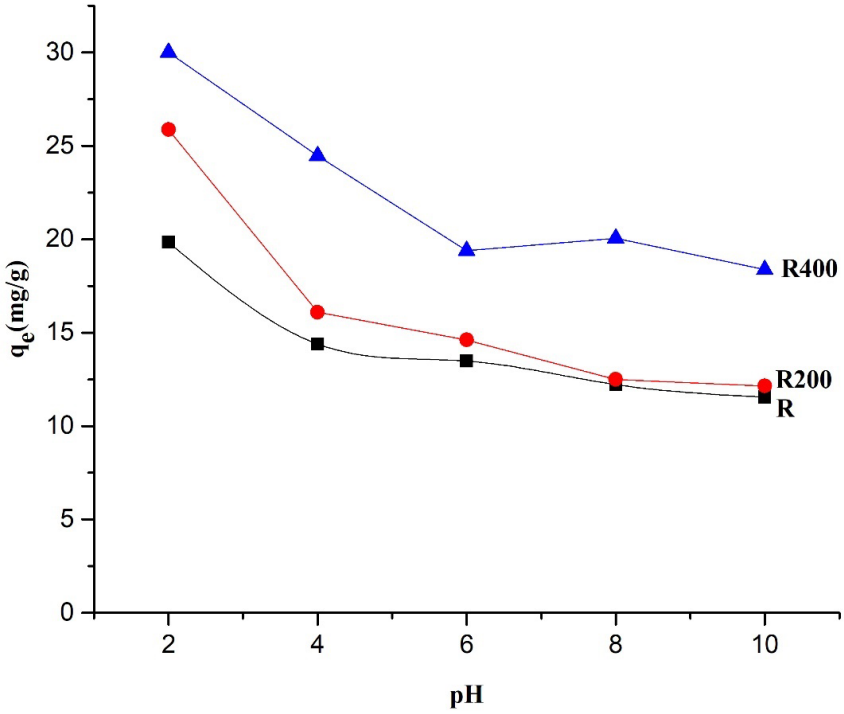


Figure 3. Adsorption evolution of IC on R, AR200 and AR400 in function of pH.

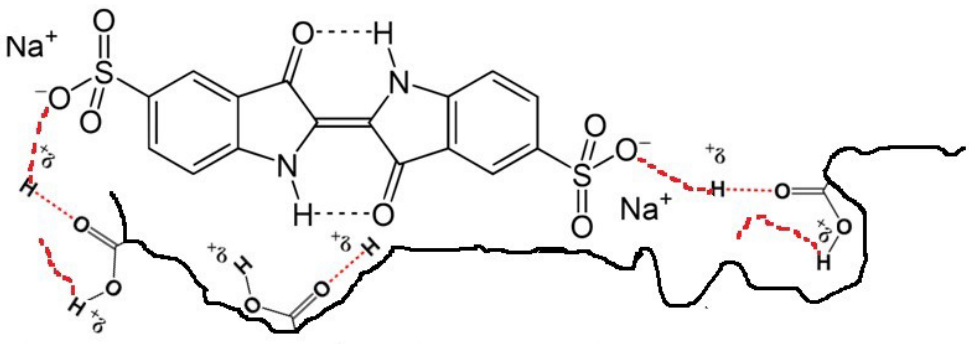


Figure 4. The mechanism adsorption of IC (pH = 2) ions onto R, AR200 and AR400 adsorbents.

3.2.2. Effect of Contact Time and Kinetic Studies

The kinetics study is essential for understanding the adsorption mechanism and determining the optimal contact time for achieving equilibrium. Figures 5–7, illustrate the effect of contact time on the adsorption of IC at concentrations of 25, 30, 40 and 50 mg/L onto three samples (R, AR200 and AR400), respectively. The results demonstrate a rapid increase in adsorption efficiency during the first 20 min, followed by a slower rate until equilibrium is reached at 50 min for all initial pollutant concentrations. This initial rapid adsorption phase is attributed to the availability of positive sites on the surface of samples, which leads to the electrostatic attraction of the anionic IC molecules. The slower adsorption rate observed for AR200 can be attributed to its lower activation level compared to AR400. The latter exhibits a more developed porosity due to activation at a higher temperature (>200 °C), which generates a greater number of active sites for adsorption. As a result, AR200 has a lower specific surface area and fewer active sites available for adsorption. In comparison, sample R also demonstrates a higher initial adsorption rate than AR200. This can be explained by the high concentration of functional groups on the surface of R. However, during thermal treatment, these functional groups gradually degrade as the temperature increases. The 200 °C stage corresponds to a phase of partial degradation of functional groups, leading to the formation of a significant number of pores. Once the majority of functional groups are decomposed, porosity further increases at 400 °C, with similar findings reported in other studies [33,34].

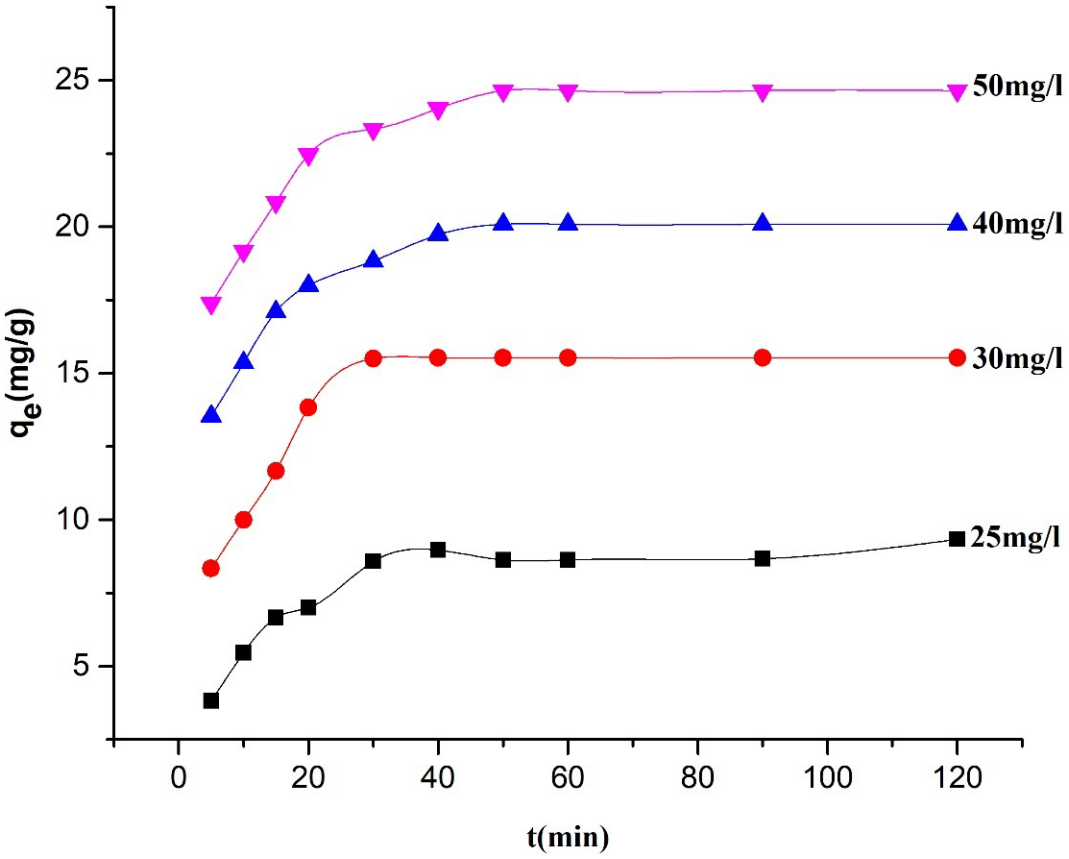


Figure 5. Adsorption evolution of IC on R in function of time.

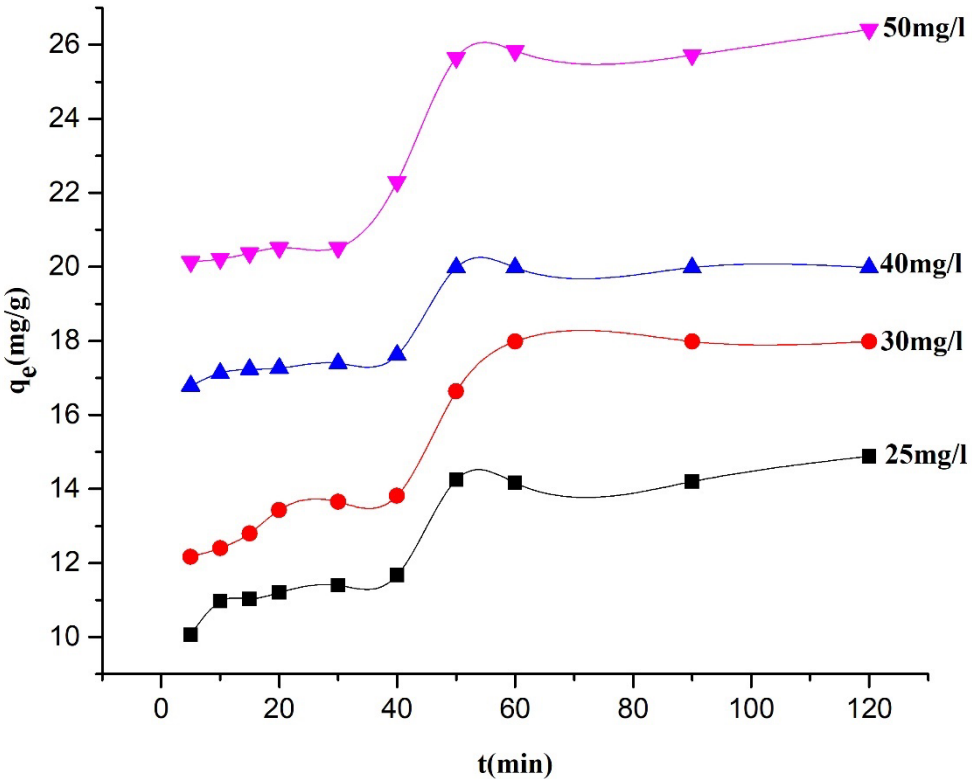


Figure 6. Adsorption evolution of IC on AR200 in function of time.

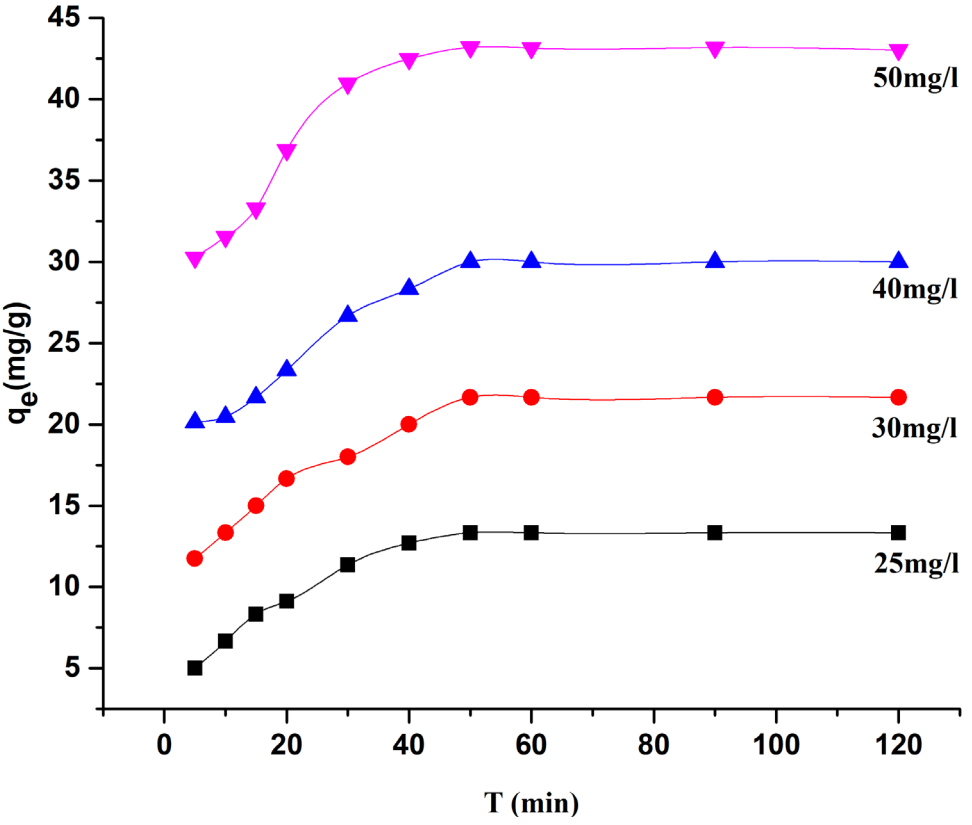


Figure 7. Adsorption evolution of IC on AR400 in function of time.

To examine the adsorption mechanism in greater detail, the time-dependent attraction efficiency of IC was analyzed. The adsorption data were evaluated using both a pseudo-first-order equation [35] and a pseudo-second-order [36] equation, as given below:

$$\log(q_e - q_t) = \log(q_e) - K \cdot t \quad (2)$$

$$\frac{t}{q_t} = \frac{1}{k_2 \cdot q_e^2} + \frac{t}{q_t} \quad (3)$$

where, q_e and qt are the adsorption efficiency (mg/g) at equilibrium and at time t, respectively. K_1 is the adsorption rate constant (min^{-1}), K_2 is the pseudo-second-order rate constant ($g \cdot mg^{-1} \cdot min^{-1}$).

The fitting results extracted from Figures 8a, 9a and 10a of pseudo-first-order and Figures 8b, 9b and 10b of pseudo-second-order are presented in Table 1 for R, AR200 and AR400. Notably, the correlation coefficient for the pseudo-second-order model is significantly higher than that for the pseudo-first-order model for the three samples. This indicates that the pseudo-second-order model is more appropriate for describing the adsorption process of IC on the R, AR200 and AR400. Additionally, the experimental values of q_e have approximately the same value of the calculated q_e compared to the calculated value q_e by pseudo-first-order. This supports the conclusion that the pseudo-second-order model better represents the kinetic behavior of the system being studied for the three samples.

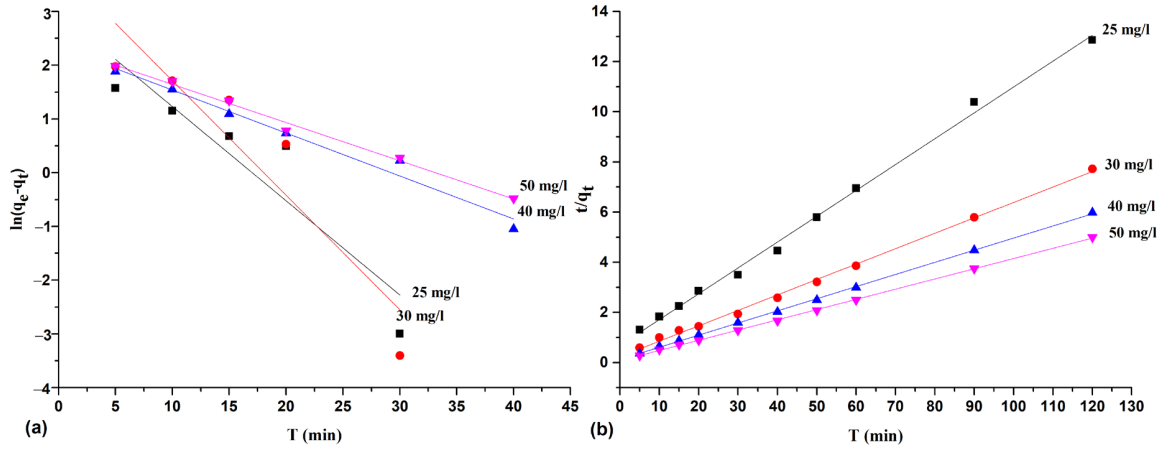


Figure 8. (**a**) Pseudo-first-order and model and (**b**) Pseudo-second-order model for R.

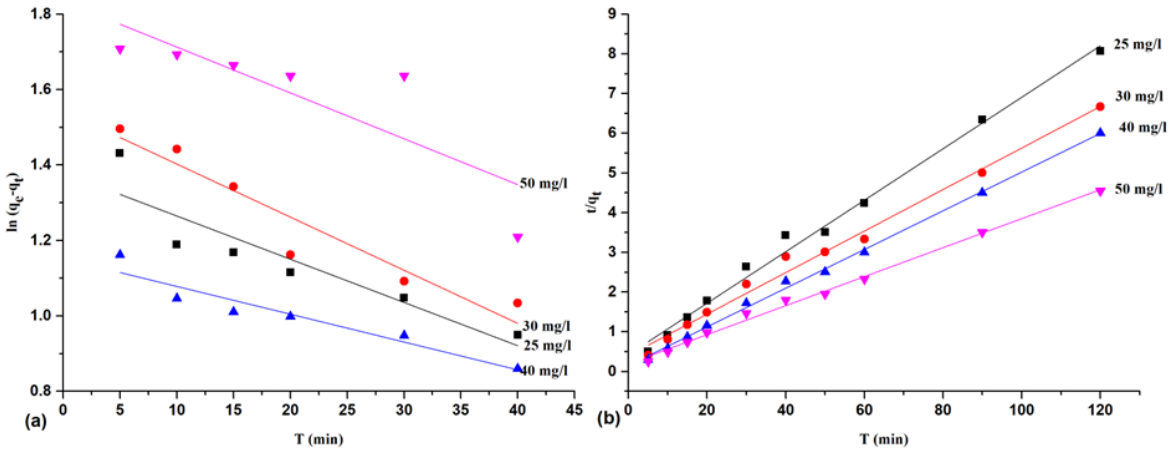


Figure 9. (**a**) Pseudo-first-order model and (**b**) Pseudo-second-order model for AR200.

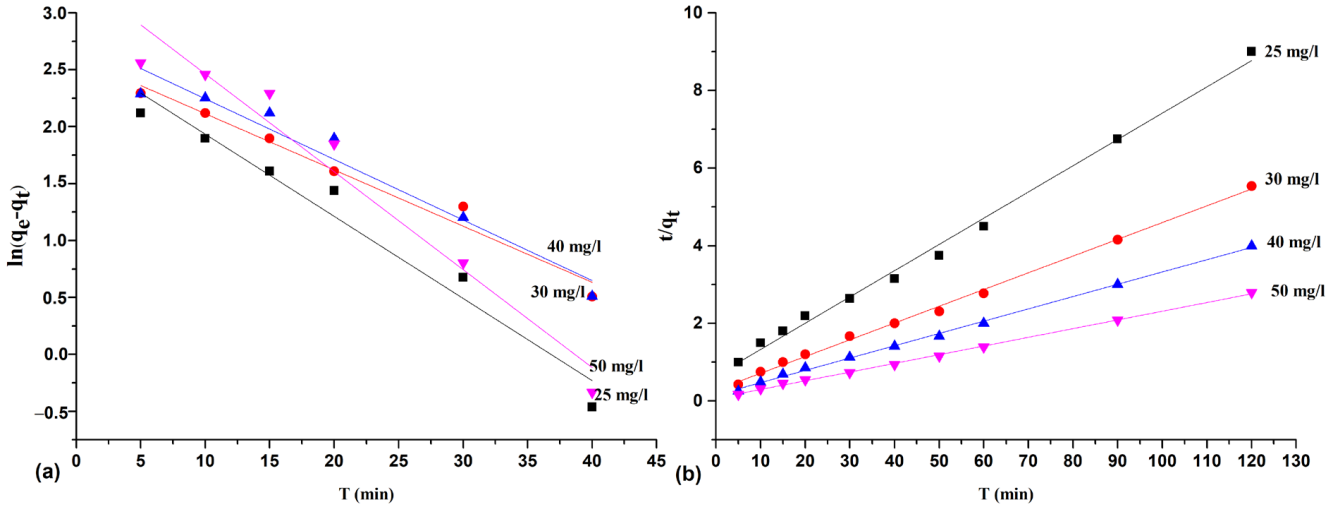


Figure 10. (**a**) Pseudo-first-order and model and (**b**) Pseudo-second-order model for AR400.

Table 1. The adsorption capacity of IC on R, AR200, and AR400 was assessed, along with constants and correlation coefficients derived from the evaluated kinetic models.

Indigo Carmine		Pseudo-First Order			Pseudo-Second Order		
	Concentration	**q_e, expr**	**q_e, calc**	**K_1**	**R^2**	**q_e, calc**	**K_2**	**R^2**
R	25	8.63	0.83	2.98	0,80	9.70	0.68	0.99
	30	15.53	0.8	3.84	0.81	16.28	0.23	0.99
	40	20.08	0.92	2.33	0.97	20.70	0.04	0.99
	50	24.03	0.93	2.35	0.99	24.57	0.07	0.99
AR 200	25	14.25	0.98	1.37	0.79	15.62	0.42	0.99
	30	16.63	0.98	1.54	0.89	19.23	0.39	0.98
	40	19.98	0.99	1.15	0.88	20.83	0.14	0.99
	50	25.65	0.98	1.83	0.62	27.77	0.19	0.99
AR 400	25	13.33	0.93	2.65	0.95	14.92	0.65	0.99
	30	21.66	0.95	2.6	0.97	23.25	0.28	0.99
	40	30	0.92	2.77	0.93	32.25	0.15	0.99
	50	43.2	0.91	3.32	0.94	45.45	0.07	0.99

3.2.3. Effect of Adsorbent Dosage

Figure 11 shows the adsorption of indigo carmine at various concentrations of R, AR200, and AR400 while maintaining a fixed dye concentration of 100 mg/L at a constant pH of 2, after allowing for an equilibrium period of 50 min. The adsorption capacity of IC adsorption rises from 67.35 to 70.75 mg/g for R, 86.13 to 87.43 mg/g for AR200 and 88.31 to 98.7 mg/g as the adsorbent concentration increases from 0.5 to 8 g/L. This increase is attributed to the greater availability of active sites on the surface of samples. However, when the adsorbent concentration exceeds 8 g/L, the percentage of dye adsorbed remains constant despite further increases in adsorbent amount. This phenomenon can be explained by the rather the availability and the strength of interaction of indigo carmine with the adsorbent. If the available dye molecules have already interacted with high-affinity sites, the adsorption process may appear saturated even though some low-affinity sites remain unoccupied.

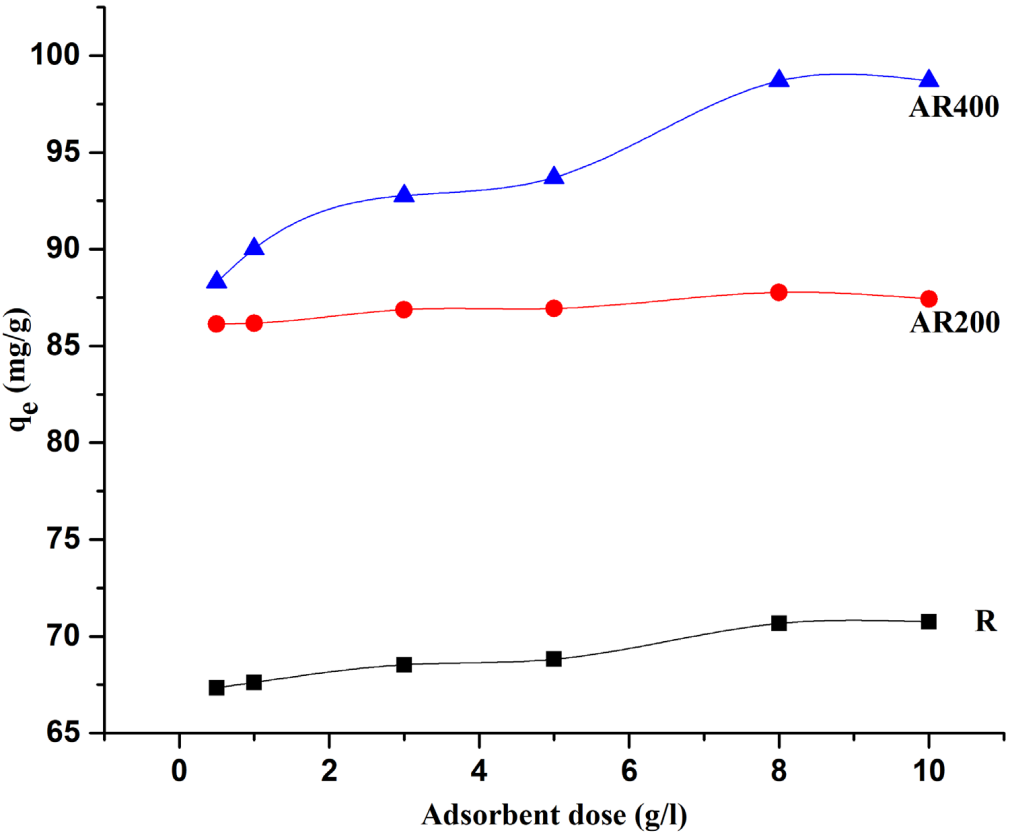


Figure 11. Adsorption evolution of IC on R, AR200 and AR400 in function of adsorbent dose.

3.2.4. Adsorption Isotherm

The configuration of isotherms represents a fundamental experimental parameter to characterize the nature of a specific adsorption phenomenon. Analyzing the shape of these isotherms provides insights into the interactions between the adsorbate and the adsorbent surface, as well as the mechanisms involved in the adsorption process. Giles and his collaborators proposed a classification of isotherms into four main categories, designated by the letters L, S, H and C [37]. Each type reflects distinct interactions and particular adsorption behaviors, thus providing valuable information on the nature of the system studied. The distribution of Indigo carmine molecules between the liquid and solid phases is illustrated by the curve shown in Figure 12 for R, AR200 and AR400. The maximum adsorption of Indigo carmine dye on samples R, AR200, and AR400 reaches capacities of 315 mg/g, 534 mg/g, and 686.7 mg/g, respectively, demonstrating significant removal efficiency. A detailed analysis of the nonlinear shape of the adsorption isotherm for these three samples categorizes the curve as an S-type isotherm according to the Giles classification. This behavior indicates cooperative interactions between the adsorbed Indigo carmine molecules, leading to increased adsorption as the solution concentration rises. Additionally, the isotherm exhibits a characteristic trend where the adsorbed amount gradually increases with the equilibrium concentration until it reaches a plateau, indicating partial saturation of the adsorption sites. After this plateau, the adsorption amount rises again, which may be attributed to molecular rearrangements or secondary interactions among the adsorbed molecules.

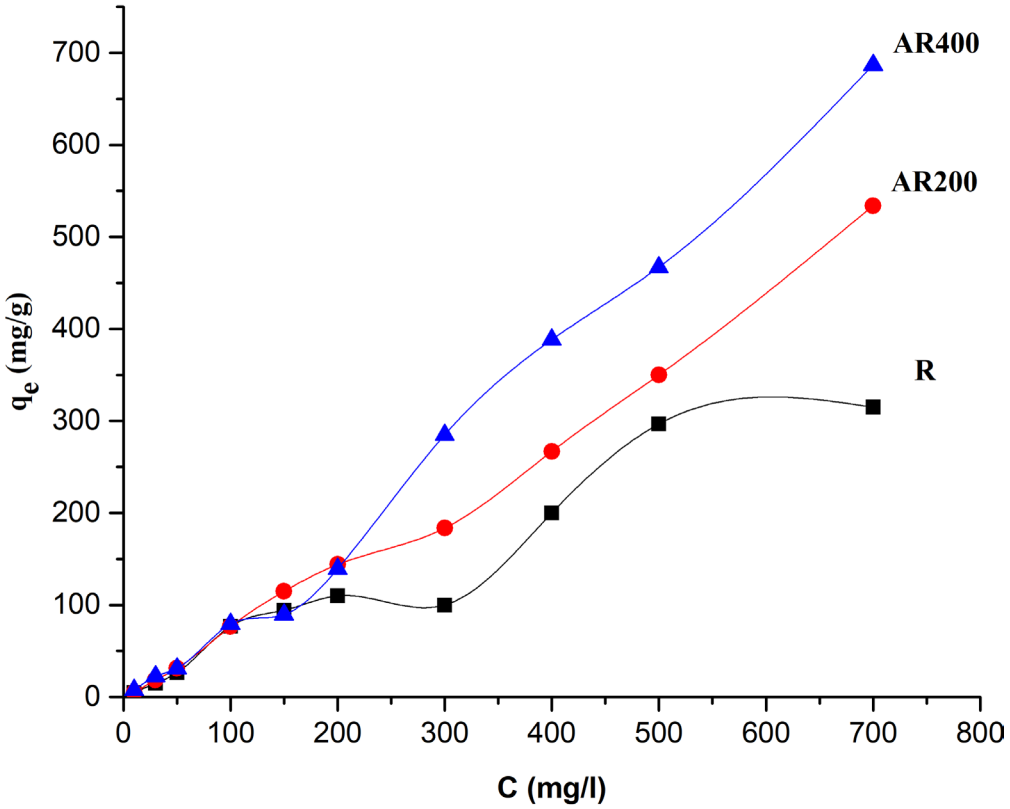


Figure 12. Nonlinear isothermal adsorption for the adsorption of IC on R, AR200 and AR400.

The observed results can be explained by the effect of increasing dye concentration, which activates more adsorption sites on the surface of the adsorbent. As the concentration rises, there is heightened competition among dye molecules for the available sites, complicating the adsorption process. In response to this competition, IC molecules may organize into successive layers on the surface of adsorbents studied (R, AR200 and AR400), indicating a multilayer adsorption mechanism. This phenomenon can be attributed to molecular interactions that favor the stacking of adsorbed molecules, resulting in the formation of multilayer structures as the concentration of the solution increases. Therefore, these findings suggest that the adsorption mechanism of IC on the samples is not limited to simple monomolecular adsorption; rather, it involves multilayer adsorption, likely due to intermolecular interactions or structural rearrangements on the adsorbent's surface. These observations highlight the complexity of the adsorption mechanisms involved in the R-IC, AR200-IC, and AR400-IC systems.

3.2.5. Isothermal Models

To identify the dye retention mechanism and determine the isotherm that most accurately describes the adsorption of dye molecules on the R, AR200, and AR400 supports, three theoretical models were applied to the experimental data obtained, namely the Langmuir model [38], Freundlich [39], Temkin [40] and Dubinin-Radushkevich [41].

The modeling of the experimental results of the IC sorption isotherms by R, AR200 and AR400 is presented in Figure 13. The values of the maximum quantity q_{max} (mg/g), the constants of the models and the correlation coefficients R^2 are deduced graphically, and grouped in Table 2. The adsorbents studied R, AR200, and AR400 demonstrated maximum adsorption capacities of 315 mg/g, 534 mg/g, and 686.7 mg/g for IC dye molecules, respectively.

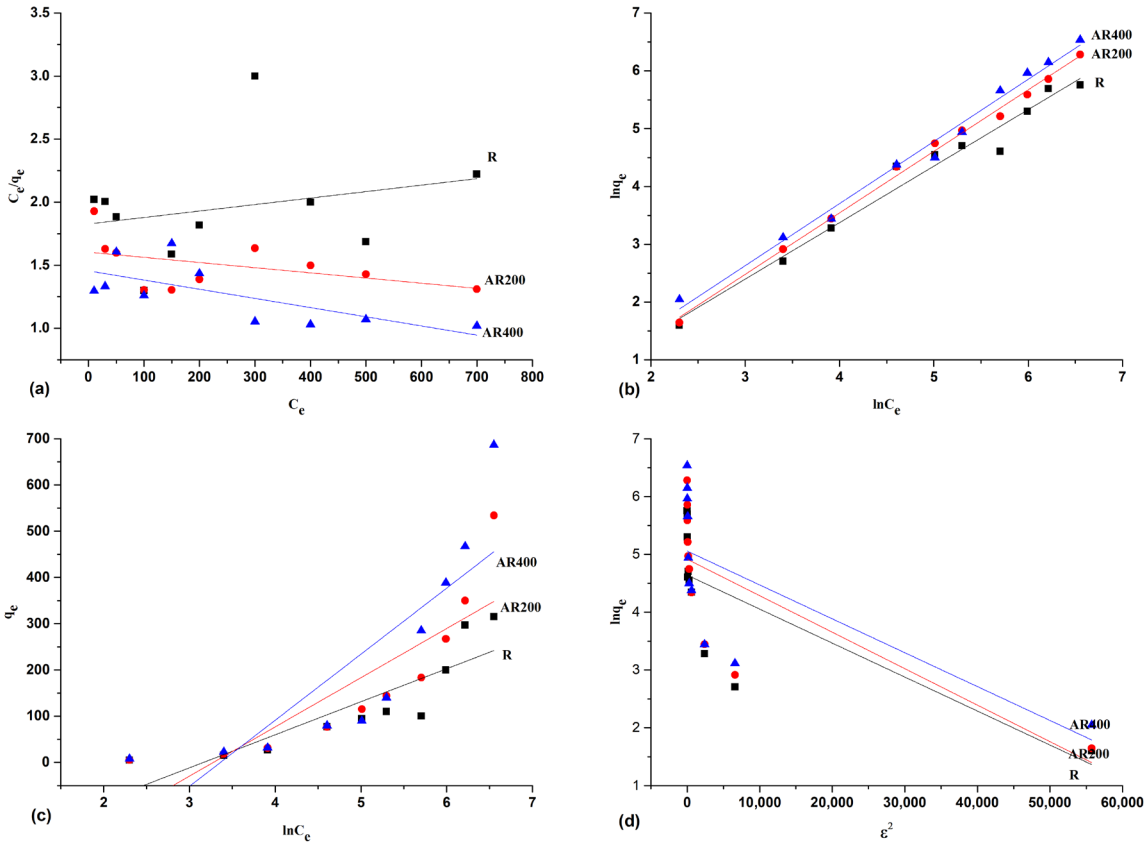


Figure 13. (**a**) Langmuir adsorption isotherm, (**b**) Freundlich adsorption isotherm, (**c**) Temkin adsorption isotherm and (**d**) Dubinin–Radushkevich isotherm of R, AR200 and AR400.

Table 2. Adsorption isotherm parameter of IR on R. AR200 and AR400.

	Models												
	Langmuir			**Freundlich**			**Temkin**			**Dubinin–Radushkevich**			
	q_{max} (mg/g)	**K_L (l/mg)**	**R^2**	**n**	**K_F (mg/g)**	**R^2**	**B**	**lnA (l/g)**	**R^2**	**q_{max}**	**E**	**K**	**R^2**
R	1960	0	0.04	1.02	0.58	0.97	71.43	−3.16	0.72	134.28	0.29	5.87	0.5
AR200	2440	0	0.12	0.93	0.48	0.99	106.41	−3.27	0.69	103.5	6.31	0.28	0.5
AR400	1370	0	0.42	0.93	0.55	0.98	142.87	−3.36	0.67	156.02	5.86	0.29	0.4

The Freundlich parameter that has been analysed shows the unique characteristics of the adsorption such as the values of K_f (Freundlich constant), n, and R2. The Freundlich parameter was calculated using Equation (4) [39]. Based on n values which lower than 1 obtained for AR200 (n = 0.939) and AR400 (n = 0.930) suggest a heterogeneous surface characterized by a distribution of adsorption energies. In this case, adsorption is more efficient at low concentrations, where high-energy sites are preferentially occupied. As the concentration increases, the remaining available sites have lower energy, making adsorption less efficient, which explains the convex curvature of the isotherm. This trend aligns with observations reported in the literature for natural adsorbents with a porous structure and diverse chemical composition [42–44].

$$\ln q_e = \ln k_f + \frac{1}{n}\ln C_e \quad (4)$$

The Langmuir isotherm model (Figure 13a) was analyzed using Equation (5) to determine key adsorption parameters, including q_{max} (maximum adsorption capacity), K (Langmuir constant), and the coefficient of determination (R^2). The corresponding Langmuir parameters are presented in Table 1.

According to the Langmuir model, adsorption occurs on a homogeneous monolayer surface, with no interaction between adsorbed molecules. The adsorption process is primarily governed by weak adsorbate-adsorbent interactions, as indicated by the value of K. An effective adsorbent is characterized by both high qmax and K values [38].

Based on the Langmuir parameters obtained for the three adsorbents: (1) AR400 exhibits a strong interaction with a moderate adsorption capacity, (2) AR200 demonstrates a high adsorption capacity but with weak interaction and (3) R shows a moderate adsorption capacity with weak interaction.

$$\frac{1}{q_e} = \frac{1}{q_{max} k_l} \frac{1}{C_e} + \frac{1}{q_{max}} \tag{5}$$

The Temkin isotherm as shown in Figure 13c was studied using Equation (6) to determine the parameters of A, B, and R^2.

$$q_e = B\ln A + B\ln C_e \tag{6}$$

The fitting curve of the Dubinin-Radushkevich adsorption isotherm (see Figure 13d) was analysed to determine the Dubinin-Radushkevich parameters such as the values of qs, E, and R^2 using Equations (7)–(9). Based on the Dubinin-Radushkevich isotherm, adsorption allows a physisorption process on the surface of the adsorbent [41].

$$\ln q_e = \ln q_{max} - \left(B\mathcal{E}^2\right) \tag{7}$$

$$\mathcal{E} = RT\ln\left(1 + \frac{1}{C_e}\right) \tag{8}$$

$$E = \frac{1}{\sqrt{2\mathcal{B}}} \tag{9}$$

According to the Dubinin-Radushkevich isotherm and the calculated average free energy presented in Table 2, the adsorption process primarily follows physisorption. Since the mean adsorption energy is less than 8 kJ/mol, this indicates that the interaction between the adsorbate molecules and the adsorbent surface occurs via weak van der Waals forces rather than chemical bonding. This confirms that the adsorption mechanism is physical in nature, as opposed to chemisorption, which typically involves higher adsorption energies (>8 kJ/mol) and stronger interactions such as covalent or ionic bonding.

The experimental data were evaluated for fit to the Langmuir, Freundlich, Temkin and Dubinin-Radushkevich isotherm models using the correlation coefficient (R^2). Among these models, the Freundlich model exhibited the correlation coefficient closest to one, indicating an excellent fit with the experimental results. This finding suggests that the Freundlich model effectively describes the adsorption behavior of IC on R, AR200, and AR400. Furthermore, this alignment supports the hypothesis of multilayer adsorption of dye molecules on the surface of R, AR200, and AR400, as indicated by the characteristics of the Freundlich model.

3.3. Comparison with Other Adsorbents

The maximum adsorption capacities (qmax) obtained in this study for R, AR200, and AR400 are presented in Table 3, along with values reported in the literature for the

adsorption of Indigo Carmine using various adsorbents. It is important to note that direct quantitative comparisons between studies are challenging due to significant variations in experimental conditions, including initial adsorbate concentration, pH, and temperature, under which these qmax values were determined.

Table 3. Comparison of maximum adsorption capacities of IC with values reported in the scientific literature.

Adsorbent	Dye	q_{max} (mg/g)	Reference	Conditions		
				T (min)	IC mg/L	pH
Waste raw	IC	315	This study	50	700	2
Activated raw at 200 °C		534				
Activated raw at 400 °C		686.7				
Activated Carbon		79.49	[45]	45	60	5.23
Rice husk ash		65.9	[46]	8	10	5.4
Cola nut shells		9.997	[47]	45	60	2
Nanoparticles from Moringa oleifera seeds		60.24	[48]	30	100	4
Chitosan/β-Cyclodextrin		1000	[49]	30	100	3

Within the context of our study conditions, the adsorbent activated at 400 °C (AR400) exhibited a higher adsorption capacity for Indigo Carmine than both the raw adsorbent R and the adsorbent activated at 200 °C (AR200). This clearly indicates that heat treatment at 400 °C significantly enhances the adsorption efficiency of this particular adsorbent for IC.

When contextualizing our results with the literature values presented in Table 3, the qmax value obtained for AR400 is comparable to some of the higher capacities reported for other materials, even considering the range of initial concentrations used across studies. While R also showed a notable capacity, particularly considering it is an untreated low-cost precursor, its direct performance comparison to other adsorbents in the table requires careful consideration of the specific experimental conditions of each study.

The results indicate that the waste generated by the fruit juice processing industry at the N'Gaous unit shows significant potential as a viable, low-cost alternative adsorbent for the remediation of wastewater contaminated with indigo carmine, with thermal activation at 400 °C notably enhancing its adsorption capacity.

4. Conclusions

The waste generated by the fruit juice processing industry at the N'Gaous unit, consisting mainly of orange peels, fibers, pulp, and seeds, were characterized using various analytical techniques. These included Fourier Transform Infrared Spectroscopy (FTIR), determination of zero-charge pH and laser scattering particle size analysis. The adsorption of indigo carmine (IC) dye onto the materials R, AR200, and AR400 was systematically studied as a function of pH, contact time, and the concentrations of both the adsorbent and the adsorbate to gain a better understanding of the involved adsorption mechanisms. The experimental results indicated that IC adsorption increased in strongly acidic media. This increase can be attributed to enhanced electrostatic interactions, consistent with the zero-charge pH values of R, AR200, and AR400 adsorbents. The pseudo-second-order kinetic model effectively described the adsorption dynamics of IC. Furthermore, the adsorption behavior of R, AR200, and AR400 transitions from monolayer adsorption at low concentrations to multilayer adsorption at high concentrations, indicating improved resistance to competition from other molecules in solution. Data fitting to the adsorption

isotherms showed that the linearized Freundlich model provided a better representation of the data than the Langmuir and Temkin models. In conclusion, this study demonstrates that activated waste generated by the fruit juice processing industry at the N'Gaous unit can serve effectively as adsorbents for removing indigo carmine from aqueous solutions. Their adsorption performance is comparable to or even superior to that of other adsorbents reported in the literature.

Author Contributions: Conceptualization: A.G. and M.K.; methodology: A.G. and M.K.; validation: All authors; formal analysis: All authors; investigation: All authors; resources: A.G. and M.K.; data curation: All authors; writing—original draft preparation: A.G. and M.K.; writing—review and editing: A.G. and M.K., K.H., C.B. and E.H.K.; visualization: All authors; supervision: K.H., C.B. and E.H.K.; project administration: K.H., C.B. and E.H.K.; funding acquisition: C.B. and E.H.K. All authors have read and agreed to the published version of the manuscript.

Funding: This research received no external funding.

Data Availability Statement: Data available on request.

Conflicts of Interest: The authors declare no conflicts of interest.

References

1. Allegra, V.; Zarbà, C.; La Via, G.; Zarbà, A.S. Why the new orange juice consumption model favors global trade and growth in orange production. *Br. Food J.* **2019**, *121*, 1954–1968. [CrossRef]
2. Milind, P.; Dev, C. Orange: Range of benefits. *Int. Res. J. Pharm.* **2012**, *3*, 52–56.
3. Gil-Izquierdo, A.; Gil, M.I.; Ferreres, F. Effect of processing techniques at industrial scale on orange juice antioxidant and beneficial health compounds. *J. Agric. Food Chem.* **2002**, *50*, 5107–5114. [CrossRef] [PubMed]
4. Agarwal, P.; Sebghatollahi, Z.; Kamal, M.; Dhyani, A.; Shrivastava, A.; Singh, K.K.; Sinha, M.; Mahato, N.; Mishra, A.K.; Baek, K.-H. Citrus essential oils in aromatherapy: Therapeutic effects and mechanisms. *Antioxidants* **2022**, *11*, 2374. [CrossRef]
5. Miles, E.A.; Calder, P.C. Effects of citrus fruit juices and their bioactive components on inflammation and immunity: A narrative review. *Front. Immunol.* **2021**, *12*, 712608. [CrossRef]
6. Zhong, G.; Nicolosi, E. Citrus origin, diffusion, and economic importance. In *The Citrus Genome*; Springer: Cham, Switzerland, 2020; pp. 5–21.
7. Sandhu, K.S.; Minhas, K.S. Oranges and citrus juices. In *Handbook of Fruits and Fruit Processing*; Blackwell Publishing: Oxford, UK, 2006; pp. 309–357.
8. Benabdelkader, M.; Saifi, R.; Saifi, H. Sustainable Agriculture in Some Arab Maghreb Countries (Morocco, Algeria, Tunisia). In *Agro-Environmental Sustainability in MENA Regions*; Springer: Cham, Switzerland, 2021; pp. 233–261.
9. Kazi-Tani, L.M. Citrus Production Conditions in Algeria: Drought and Irrigation Issues. In *Transformation Towards Circular Food Systems: Sustainable, Smart and Resilient Citrus Supply Chains in Mediterranean Areas*; Springer: Cham, Switzerland, 2024; pp. 61–83.
10. Etebu, E.; Nwauzoma, A. A review on sweet orange (*Citrus sinensis* L. Osbeck): Health, diseases and management. *Am. J. Res. Commun.* **2014**, *2*, 33–70.
11. Chavan, P.; Singh, A.K.; Kaur, G. Recent progress in the utilization of industrial waste and by-products of citrus fruits: A review. *J. Food Process Eng.* **2018**, *41*, e12895. [CrossRef]
12. Rezzadori, K.; Benedetti, S.; Amante, E. Proposals for the residues recovery: Orange waste as raw material for new products. *Food Bioprod. Process.* **2012**, *90*, 606–614. [CrossRef]
13. Ortiz, D.; Batuecas, E.; Orrego, C.; Rodríguez, L.J.; Camelin, E.; Fino, D. Sustainable management of peel waste in the small-scale orange juice industries: A Colombian case study. *J. Clean. Prod.* **2020**, *265*, 121587. [CrossRef]
14. Sial, T.A.; Lan, Z.; Khan, M.N.; Zhao, Y.; Kumbhar, F.; Liu, J.; Zhang, A.; Hill, R.L.; Lahori, A.H.; Memon, M. Evaluation of orange peel waste and its biochar on greenhouse gas emissions and soil biochemical properties within a loess soil. *Waste Manag.* **2019**, *87*, 125–134. [CrossRef]
15. Babuji, P.; Thirumalaisamy, S.; Duraisamy, K.; Periyasamy, G. Human health risks due to exposure to water pollution: A review. *Water* **2023**, *15*, 2532. [CrossRef]
16. Youvan, D.C. The Living Waters of Earth: How Every Drop Has Passed Through Life Millions of Times. 2024. Available online: https://www.researchgate.net/publication/385509601_The_Living_Waters_of_Earth_How_Every_Drop_Has_Passed_Through_Life_Millions_of_Times (accessed on 26 May 2025).
17. Ristea, M.-E.; Zarnescu, O. Indigo carmine: Between necessity and concern. *J. Xenobiotics* **2023**, *13*, 509–528. [CrossRef]

18. Islam, T.; Repon, M.R.; Islam, T.; Sarwar, Z.; Rahman, M.M. Impact of textile dyes on health and ecosystem: A review of structure, causes, and potential solutions. *Environ. Sci. Pollut. Res.* **2023**, *30*, 9207–9242. [CrossRef]
19. Sonune, A.; Ghate, R. Developments in wastewater treatment methods. *Desalination* **2004**, *167*, 55–63. [CrossRef]
20. Rashid, R.; Shafiq, I.; Akhter, P.; Iqbal, M.J.; Hussain, M. A state-of-the-art review on wastewater treatment techniques: The effectiveness of adsorption method. *Environ. Sci. Pollut. Res.* **2021**, *28*, 9050–9066. [CrossRef]
21. Yazid, H.; Bouzid, T.; Regti, A.; El Himri, M.; El Haddad, M. Experimental and DFT insights into the adsorption competition of two cationic dyes on activated carbon derived from walnut shells in aqueous solutions. *Environ. Nanotechnol. Monit. Manag.* **2024**, *21*, 100940. [CrossRef]
22. Ahmad, M.; Lee, S.S.; Dou, X.; Mohan, D.; Sung, J.-K.; Yang, J.E.; Ok, Y.S. Effects of pyrolysis temperature on soybean stover-and peanut shell-derived biochar properties and TCE adsorption in water. *Bioresour. Technol.* **2012**, *118*, 536–544. [CrossRef]
23. Silverstein, R.; Webster, E.; Kiley, D. *Spectrometric Identification of Organic Compounds*, 7th ed.; John Wilye and Sons: New York, NY, USA, 2005.
24. de Carvalho, H.P.; Huang, J.; Zhao, M.; Liu, G.; Dong, L.; Liu, X. Improvement of Methylene Blue removal by electrocoagulation/banana peel adsorption coupling in a batch system. *Alex. Eng. J.* **2015**, *54*, 777–786. [CrossRef]
25. Yang, H.; Yan, R.; Chen, H.; Lee, D.H.; Zheng, C. Characteristics of hemicellulose, cellulose and lignin pyrolysis. *Fuel* **2007**, *86*, 1781–1788. [CrossRef]
26. Santos, C.M.; Dweck, J.; Viotto, R.S.; Rosa, A.H.; de Morais, L.C. Application of orange peel waste in the production of solid biofuels and biosorbents. *Bioresour. Technol.* **2015**, *196*, 469–479. [CrossRef]
27. Kacurakova, M.; Capek, P.; Sasinkova, V.; Wellner, N.; Ebringerova, A. FT-IR study of plant cell wall model compounds: Pectic polysaccharides and hemicelluloses. *Carbohydr. Polym.* **2000**, *43*, 195–203. [CrossRef]
28. Mullen, C.A.; Boateng, A.A.; Goldberg, N.M.; Lima, I.M.; Laird, D.A.; Hicks, K.B. Bio-oil and bio-char production from corn cobs and stover by fast pyrolysis. *Biomass Bioenergy* **2010**, *34*, 67–74. [CrossRef]
29. Khormaei, M.; Nasernejad, B.; Edrisi, M.; Eslamzadeh, T. Copper biosorption from aqueous solutions by sour orange residue. *J. Hazard. Mater.* **2007**, *149*, 269–274. [CrossRef] [PubMed]
30. Keiluweit, M.; Nico, P.S.; Johnson, M.G.; Kleber, M. Dynamic molecular structure of plant biomass-derived black carbon (biochar). *Environ. Sci. Technol.* **2010**, *44*, 1247–1253. [CrossRef]
31. Banerjee, S.; Dubey, S.; Gautam, R.K.; Chattopadhyaya, M.; Sharma, Y.C. Adsorption characteristics of alumina nanoparticles for the removal of hazardous dye, Orange G from aqueous solutions. *Arab. J. Chem.* **2019**, *12*, 5339–5354. [CrossRef]
32. Doke, K.; Yusufi, M.; Joseph, R.; Khan, E. Comparative adsorption of crystal violet and congo red onto ZnCl2 activated carbon. *J. Dispers. Sci. Technol.* **2016**, *37*, 1671–1681. [CrossRef]
33. El Gheriany, I.A.; El Saqa, F.A.; Amer, A.A.E.R.; Hussein, M. Oil spill sorption capacity of raw and thermally modified orange peel waste. *Alex. Eng. J.* **2020**, *59*, 925–932. [CrossRef]
34. Zapata, B.; Balmaseda, J.; Fregoso-Israel, E.; Torres-García, E. Thermo-kinetics study of orange peel in air. *J. Therm. Anal. Calorim.* **2009**, *98*, 309–315. [CrossRef]
35. Lagergren, E.; Over, P. Comparing interactive information retrieval systems across sites: The TREC-6 interactive track matrix experiment. In Proceedings of the 21st Annual International ACM SIGIR Conference on Research and Development in Information Retrieval, Melbourne, Australia, 24–28 August 1998; pp. 164–172.
36. Ho, Y.-S.; McKay, G. Pseudo-second order model for sorption processes. *Process Biochem.* **1999**, *34*, 451–465. [CrossRef]
37. Giles, C.H.; D'Silva, A.P.; Easton, I.A. A general treatment and classification of the solute adsorption isotherm part. II. Experimental interpretation. *J. Colloid Interface Sci.* **1974**, *47*, 766–778. [CrossRef]
38. Langmuir, I. The adsorption of gases on plane surfaces of glass, mica and platinum. *J. Am. Chem. Soc.* **1918**, *40*, 1361–1403. [CrossRef]
39. Freundlich, H. Über die adsorption in lösungen. *Z. Für Phys. Chem.* **1907**, *57*, 385–470. [CrossRef]
40. Eriksson, M.; Lundström, I.; Ekedahl, L.-G. A model of the Temkin isotherm behavior for hydrogen adsorption at Pd–SiO_2 interfaces. *J. Appl. Phys.* **1997**, *82*, 3143–3146. [CrossRef]
41. Ragadhita, R.; Nandiyanto, A.B.D. Curcumin adsorption on zinc imidazole framework-8 particles: Isotherm adsorption using Langmuir, Freundlich, Temkin, and Dubinin-Radushkevich models. *J. Eng. Sci. Technol.* **2022**, *17*, 1078–1089.
42. Kaya, E.M.Ö.; Özcan, A.S.; Gök, Ö.; Özcan, A. Adsorption kinetics and isotherm parameters of naphthalene onto natural-and chemically modified bentonite from aqueous solutions. *Adsorption* **2013**, *19*, 879–888. [CrossRef]
43. Chen, X.-T.; Yu, P.-F.; Xiang, L.; Zhao, H.-M.; Li, Y.-W.; Li, H.; Zhang, X.-Y.; Cai, Q.-Y.; Mo, C.-H.; Wong, M.H. Dynamics, thermodynamics, and mechanism of perfluorooctane sulfonate (PFOS) sorption to various soil particle-size fractions of paddy soil. *Ecotoxicol. Environ. Saf.* **2020**, *206*, 111105. [CrossRef]
44. Falaki, Z.; Bashiri, H. Preparing an adsorbent from the unused solid waste of Rosewater extraction for high efficient removal of Crystal Violet. *J. Iran. Chem. Soc.* **2021**, *18*, 2689–2702. [CrossRef]

45. Harrache, Z.; Abbas, M.; Aksil, T.; Trari, M. Thermodynamic and kinetics studies on adsorption of Indigo Carmine from aqueous solution by activated carbon. *Microchem. J.* **2019**, *144*, 180–189. [CrossRef]
46. Lakshmi, U.R.; Srivastava, V.C.; Mall, I.D.; Lataye, D.H. Rice husk ash as an effective adsorbent: Evaluation of adsorptive characteristics for Indigo Carmine dye. *J. Environ. Manag.* **2009**, *90*, 710–720. [CrossRef]
47. Odogu, A.N.; Daouda, K.; Desiré, B.B.P.; Nsami, N.J.; Mbadcam, K.J. Removal of Indigo Carmine Dye (IC) by Batch Adsorption Method onto Dried Cola Nut Shells and Its Active Carbon from Aqueous Medium. *Int. J. Eng. Sci. Res. Technol.* **2016**, *5*, 874–887.
48. El-Kammah, M.; Elkhatib, E.; Gouveia, S.; Cameselle, C.; Aboukila, E. Enhanced removal of Indigo Carmine dye from textile effluent using green cost-efficient nanomaterial: Adsorption, kinetics, thermodynamics and mechanisms. *Sustain. Chem. Pharm.* **2022**, *29*, 100753. [CrossRef]
49. Kekes, T.; Tzia, C. Adsorption of indigo carmine on functional chitosan and β-cyclodextrin/chitosan beads: Equilibrium, kinetics and mechanism studies. *J. Environ. Manag.* **2020**, *262*, 110372. [CrossRef] [PubMed]

Disclaimer/Publisher's Note: The statements, opinions and data contained in all publications are solely those of the individual author(s) and contributor(s) and not of MDPI and/or the editor(s). MDPI and/or the editor(s) disclaim responsibility for any injury to people or property resulting from any ideas, methods, instructions or products referred to in the content.